Image reconstruction at Cambridge University

Fabien Baron, John S. Young

University of Cambridge, Cavendish Laboratory, JJ Thomson Avenue,
Cambridge CB3 0HE, United Kingdom

ABSTRACT

We present the recent results in image reconstruction obtained with the University of Cambridge's software package BSMEM (BiSpectrum Maximum Entropy Method). We also evaluate the performance of BSMEM reconstructions for several datasets susceptible to render the reconstruction process harder: with missing power-spectrum or bispectrum points, low Signal-to-Noise ratio on visibility phases or visibility amplitudes, or problematic source morphologies (important amount of resolved flux, centro-symmetry). Interferometer configurations with 4, 6, 8 and 15 telescopes are examined.

Keywords: Image reconstruction, Interferometry

1. INTRODUCTION

Future interferometric instruments will benefit from increased *uv* coverage offered by new facilities (Magdalena Ridge Observatory Interferometer, OHANA) or existing ones (simultaneous use of the ATs and the UTs at the VLTI). Consequently, model-independent imaging from interferometric data, which quality heavily depends on the *uv* coverage, is to become increasingly important in terms of scientific output.

The SPIE Interferometry Imaging Beauty Contests, which took place in 2004,[1] 2006[2] and 2008 have been welcome opportunities to demonstrate that model-independent imaging can be powerful even at low SNR. The majority of image reconstruction softwares rely on similar approaches (iterative process with minimization of a criterion), even if the implementations may differ. Recent improvements in the field include the introduction of a myopic model of the telescope aberrations[3,4] and the use of stochastic techniques such as Markov Chains.[5]

We present in section 2 Cambridge's image reconstruction software, BSMEM, an implementation of the classic Maximum Entropy Method. As BSMEM won the two first Beauty Contests and came second in the latest one, its performance can be seen as representative of what image reconstruction softwares are currently able to achieve.

The Beauty Contest relies on simulated datasets to evaluate the candidates. While those datasets are certainly not easy, quality images can be reconstructed without trouble. Real data may differ in that they may not allow perfect images to be retrieved. To assess BSMEM's robustness we conducted several simulations on various representative difficult datasets, presented in section3. They encompass datasets with low *uv* coverage (as can be found in facilities not primarily intended for imaging), low SNR or missing bispectrum points, as well as potential issues arising from the source morphology (large amount of resolved flux or centrosymmetry).

We present the main results of these simulations in section 4 and we underline several key principles that the observer should remember before using a model-independent image reconstruction software with such noisy datasets.

2. BSMEM

Cambridge's software package has been dubbed BSMEM to stand for BiSpectrum Maximum Entropy Method. It was first written in 1992 to demonstrate image reconstruction from optical aperture synthesis data.[6] It applies a fully Bayesian approach to the inverse problem of finding the most probable image given the evidence, making use of the Maximum Entropy approach to maximize the inference of an image. This approach, described in section 2, is now classic in image reconstruction for optical and infrared interferometry. BSMEM is now available freely to the interferometry community at `http://www.mrao.cam.ac.uk/research/OAS/bsmem.html`.

Further author information: Fabien Baron: E-mail: baron@mrao.cam.ac.uk, Telephone: +44 1223 766476

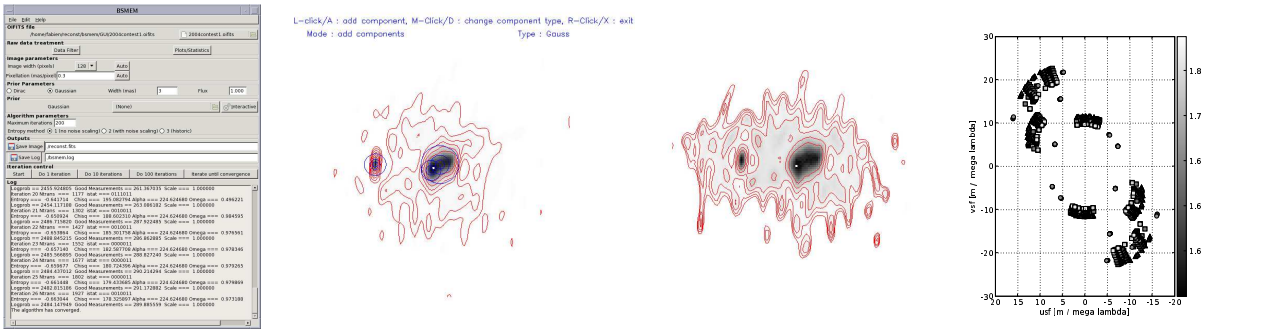

Figure 1. BSMEM user-interface. From left to right: the main window, creation of a new starting model over the current reconstruction, standard deviation of the posterior probability, and an OIPLOT window.

2.1 The algorithm behind BSMEM

2.1.1 A Bayesian approach

BSMEM reconstructs an image $\boldsymbol{I}$ from an OIFITS file which contains a set $\boldsymbol{D}$ of data points potentially composed of complex visibilities, powerspectra, triple amplitudes, closure phases and their associated measurement noises. For simplicity we will not consider the presence of complex visibilities in this paper. We only assume the data to be composed of powerspectrum points $\{P_1, P_2, \dots P_{N_{\rm pow}}\}$ as well as triple amplitudes $\{T_1, T_2, \dots T_{N_{\rm trip}}\}$ and closure phases $\{C_1, C_2, \dots C_{N_{\rm clos}}\}$. While the numbers of triple amplitudes and closure phases may not match, when reading the OIFITS file BSMEM actually reforms complete bispectrum data $\{B_1, B_2, \dots B_{N_{\rm bis}}\}$ with $N_{\rm bis} = \text{argmax}\{N_{\rm trip}, N_{\rm clos}\}$. For each bispectrum point thus created, if either the corresponding closure phase or the triple amplitude is missing, then BSMEM flags the point so that it may be treated appropriately during further analysis. The noise is assumed to be Gaussian, and the OIFITS file contains the variances for all measurements (e.g. $\sigma^2_{P_n}$, $\sigma^2_{T_n}$ and $\sigma^2_{C_n}$).

BSMEM reconstruction algorithm is based on the Bayesian equation:

$$\Pr(\boldsymbol{I}|\boldsymbol{D}) = \frac{\Pr(\boldsymbol{I})\Pr(\boldsymbol{D}|\boldsymbol{I})}{\Pr(\boldsymbol{D})} \quad , \tag{1}$$

where $\Pr(\boldsymbol{I}|\boldsymbol{D})$ is the posterior probability density (also called inference), $\Pr(\boldsymbol{D}|\boldsymbol{I})$ is the likelihood, $\Pr(\boldsymbol{I})$ the prior, and $\Pr(\boldsymbol{D})$ the evidence. BSMEM uses an iterative method to maximize the posterior probability, in order to obtain the most likely image constrained by the prior.

2.1.2 BSMEM likelihood

As we deal with Gaussian white noise, the likelihood is simply:

$$\Pr(\boldsymbol{D}|\boldsymbol{I}) \propto \exp\left[-\frac{\chi^2_{\boldsymbol{D}}(\boldsymbol{I})}{2}\right] \quad . \tag{2}$$

The first step toward computing $\chi^2_{\boldsymbol{D}}$ is to derive all powerspectra P_n and bispectra B_n from the image $\boldsymbol{I}$. This is straightforward and will not be detailed here. Then $\chi^2_{\boldsymbol{D}}$ is expressed as the sum of two least-square criteria on the powerspectra and bispectra:

$$\chi^2_{\boldsymbol{D}} = \sum_{n=1}^{N_{\rm pow}} J_n^{\rm pow} + \sum_{n=1}^{N_{\rm bis}} J_n^{\rm Bis} \quad , \tag{3}$$

with

$$J_n^{\rm pow} = \left(\frac{P_n - P_n^{\rm data}}{\sigma_{P_n}}\right)^2 \quad , \tag{4}$$

and

$$J_n^{\mathrm{Bis}} = \left(\frac{\mathcal{R}\left[(B_n - B_n^{\mathrm{data}}) \frac{B_d^{\mathrm{data}\,*}}{\left|B_d^{\mathrm{data}}\right|} \right]}{\sigma_n^{\mathrm{rad}}} \right)^2 + \left(\frac{\mathcal{I}\left[(B_n - B_n^{\mathrm{data}}) \frac{B_d^{\mathrm{data}\,*}}{\left|B_d^{\mathrm{data}}\right|} \right]}{\sigma_n^{\mathrm{tan}}} \right)^2 \quad . \tag{5}$$

Note that we do not use a simple χ^2 on the bispectrum. The reason is that the noise statitics is Gaussian on both its amplitude and phase, resulting in a banana-shaped noise cloud on the bispectrum itself. Using a simple χ^2 directly on the bispectrum would create a bias, and such a criterion would be tricky to minimize as it is non-convex.

It can be shown that before comparison to the data, each tentative bispectrum vector B_n has to be rotated by an angle equal to the opposite of the closure phase data. Then a convex approximation of the bispectrum noise cloud can be realized by an elliptical cloud along the radial and tangential axis of the bispectrum data point. The standard deviations on the radial and tangential parts of the bispectrum take the form:

$$\sigma_n^{\mathrm{rad}\,2} = \frac{1 + e^{-\sigma_{C_n}^2}}{2} T_n^2 + \frac{1 + e^{-\sigma_{C_n}^2}}{2} \sigma_{T_n}^2 \quad , \tag{6}$$

and

$$\sigma_n^{\mathrm{tan}\,2} = \frac{1 - e^{-\sigma_{C_n}^2}}{2} T_n^2 + \frac{1 - e^{-\sigma_{C_n}^2}}{2} \sigma_{T_n}^2 \quad . \tag{7}$$

In BSMEM those deviation are evaluated once, using the OIFITS data only (though it may be useful to update their values when converging toward a solution). It can be shown that the elliptic approximation is not biased radially as long as the triple amplitude is low compared to unity (which is nearly always the case). Note that a similar approach has also been used recently by Meimon et al.,[3] but for image reconstruction from complex visibilities.

2.1.3 BSMEM prior

The regularization prior in image reconstruction is classically shown to take the form:

$$\Pr(\boldsymbol{D}|\boldsymbol{I}) \propto \exp\left[\alpha H(\boldsymbol{I})\right] \quad , \tag{8}$$

with $\alpha \in \mathbb{R}$ so that maximising the inference becomes a problem of minimising the criterion:

$$J(\boldsymbol{I}) = \chi^2_{\boldsymbol{D}}(\boldsymbol{I}) - \alpha H(\boldsymbol{I}) \quad , \tag{9}$$

where is α is called the regularization constant and H the prior (or regularization function). The maximum a posteriori image $\widetilde{\boldsymbol{I}}$ reconstructed by BSMEM is then given by:

$$\widetilde{\boldsymbol{I}} = \mathrm{argmax}_{I \in \mathbb{R}^N}\, J(\boldsymbol{I}) \quad . \tag{10}$$

BSMEM uses the Maximum Entropy Method (MEM) and thus considers regularization functions which measure the entropy of the image. Maximising the entropy ensures that the information contained in the reconstructed image is the minimum available, while the likelihood term still imposes compatibility with the data. While several entropy functions H are commonly used in the literature, and BSMEM currently only implements the Gull and Skilling one:[7]

$$H(\boldsymbol{I}) = \sum_{k=1}^{N} (\boldsymbol{I}_k - \boldsymbol{M}_k) - \boldsymbol{I}_k \log\left(\frac{\boldsymbol{I}_k}{\boldsymbol{M}_k}\right) \quad , \tag{11}$$

where $\boldsymbol{M}$ is a given prior image and the subscript k gives the value of the kth pixel. This entropy function can be seen as the sum of two terms, one being the total flux difference between the reconstructed image and the model, and the other a Kullback-Leibler divergence between image and model. In practise the model we use is either

a Gaussian, a uniform disk, or a Dirac centered in the field of view as those conveniently allow to artificially fix the center of the reconstruction (the fit on the bispectrum and powerspectrum data is translation-invariant). This type of starting models also acts as a support constrain by an penalising the presence of flux far from the center of the image.

As Eq. 9 demonstrates, the balance between the χ^2 and the entropy function depends on the hyperparameter α. Choosing an adequate hyperparameter is sometimes a difficult task for the user and so BSMEM implements an automatic Bayesian estimation of the hyperparameter. The prior $\Pr(\alpha)$ is a cut-off Jeffreys prior and the evidence $\Pr(\boldsymbol{D}|\alpha)$ is sampled to determine the most likely α. The reconstruction is then totally unsupervised and J is minimised using the non-linear conjugate gradient method implemented in the MEMSYS library.[8]

2.2 Other BSMEM features

Since 1992 multiple improvements have been brought to BSMEM. It has partly been ported to C, has gained compatibility with the OIFITS format,[9] the number of reconstruction options and the user interface have been improved and expanded. The latest version, described in this paper, includes a Python/GTK GUI and the integration of the OIPLOT libraries from Thureau et al.[10] with easy plot export and limited model-fitting options. This version also has been streamlined so that new users may use it without prior knowledge of image reconstruction: an automatic mode adjusts the reconstruction parameters such as the pixellation, the field of view, the regularization constant and the starting model. There are several ways in BSMEM for the user to define its starting model: by reading a bitmap file, by using a component description of the source, or even by drawing it with the mouse directly over the current reconstruction.

A very useful new feature is the ability to sample the posterior probability distribution close to the reconstructed image. This allows to compute statistics on a set of most probable images such as minimum/maximum levels, mean image, median image or the standard deviation. This latter allows to assign error bars to each pixel of the reconstruction, and thus to associate a level of confidence to the image features.

BSMEM is distributed under the LGPL license to any member of the interferometric community contacting us.[11] It can be compiled under Linux, Solaris, MacOS, Windows XP/Vista. As the BSMEM userbase is quickly growing, a mailing list has recently been started.

Several paths are explored to further improve BSMEM performance, flexibility and usability. Among the studied options are the choice of several regularization functions (L1, L2, L1L2 norms, support constrains, multiscale entropy regularizers), the explicit introduction of intrinsic correlation functions, and a bi-model approach with a separated treatment of extended components and point sources. Support for any future additions to the OIFITS format (e.g. possibly closure amplitudes) will also be added. Finally, support for multiwavelengths datasets with the simultaneous reconstruction of several channels is also one of our primary goals.

3. SIMULATION SETUP

In theory BSMEM has several advantages over the old phase self-calibration procedures that used to be applied in interferometry. The latter failed in most cases where the data was mostly composed of the powerspectrum with only a very few bispectrum points, as it relied on the bispectrum and powerspectrum components sharing common uv points. On the contrary BSMEM independently exploits the powerspectrum points, the triple product amplitudes, and the phase closures and it can handle all types of data sparseness (such as the frequent case of missing closures). The following simulations allowed us to verify the validity and usefulness of this approach.

3.1 Fake data generation

Let us describe here the procedure which was followed to create of the fake data sets. First four different array configurations have been used and are presented on figure 2. The first one is the well-known VLTI configuration with four UTs telescopes, while others are configurations with more telescopes. Bootstrapping capability is a strong advocacy for Y arrays, so such configurations are commonly considered for future interferometers. Here the 6 telescope configuration is close to what could be obtained with the Magdalena Ridge Observatory Phase A. The second generation VLTI instrument VSI is planned to get a 8 telescope configuration, and our 8 telescope

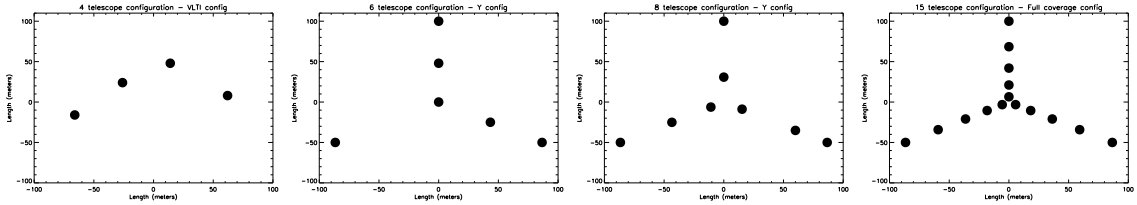

Figure 2. Array configurations, from left to right: VLTI configuration, Y configurations with 6 (MROI phase A), 8 (MROI between phase A and B), and 15 telescopes (exhaustive coverage).

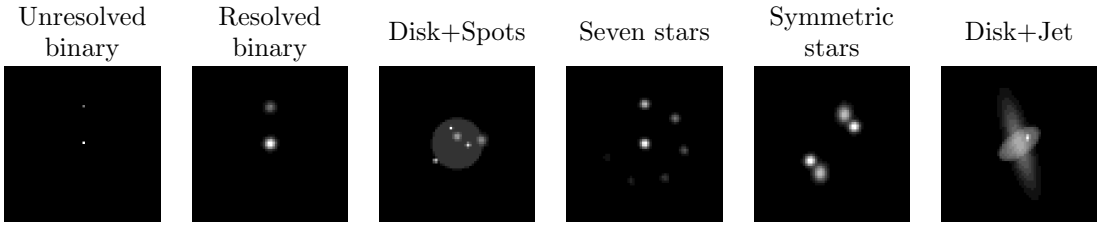

Figure 3. The sources for the simulations. They were chosen to evaluate the potential of model-independent image reconstruction on target with specific characteristics (resolved and unresolved, symmetric/asymmetric, with or without extended components).

configuration reflects this point. Most interferometers are not especially designed with imaging in mind, so the chosen configurations are not especially optimised for best imaging performance. On the contrary they are meant to give average and representative results: as a result the *uv* plane is decently covered by the 6 and 8 telescope arrays but not completely. On the other hand, the 15 telescope case is meant to be the example of an exhaustive coverage of the *uv* plane. This latter configuration allows to study the importance of the object shape on reconstruction capabilities as the differences arising from the reconstruction process cannot be attributed to a lack of *uv* coverage but to a genuine MEM behaviour with respect to the object. All Y configurations possess maximum baselines of about 170 meters, which is slightly greater than the maximum baseline of the VLTI one (about 130 m), but represents well the increased goals for next-generation interferometers. The reader will understand that our goal was not to compare the VLTI to another array configuration of the same resolution, but more to a state-of-the-art interferometer, and then determine in which cases the increased *uv* coverage would bring major improvements.

To be consistent with existing instruments, all tests have been run in the near infrared bands ($\lambda \simeq 1.0\mu$m). The typical baseline range for the simulated instruments was around $40 - 200$m, thus approximatively defining a practical limit between resolved (> 1.0 mas) and unresolved (< 0.1 mas) simulated objects. The simulated observation strategy consisted in 16 acquisitions every 15 minutes, so 4 hours total time. During each acquisition all available bispectrum and powerspectrum were measured.

Six test sources have been selected and are presented on Fig. 3. They are not meant to be representative of real objects: they are difficult cases tailored to test the reconstruction behavior and understand the potential shortcomings of BSMEM or similar programs (more realistic targets are analysed in the paper by Filho et al. in these Proceedings). The flux levels were chosen to match those of a K=10 unresolved target. The amount of resolved flux and symmetry of the source are expected to have a major influence on the performance.

From left to right in Fig. 3, source 1 is the simplest test case, an unresolved binary of flux ratio 1:5, separation 3 mas, which constitutes our reference "easy" source. Source 2 is a resolved binary of flux ratio 1:5, same size 0.5 mas (Gaussian functions), and separation 3 mas. Source 3 is a a typical source, a resolved stellar disk with several resolved or barely resolved spots at its surface. Source 4 is a object composed of seven resolved (0.4 mas) sources of different fluxes. With the brightest star taken as reference, the flux ratios are 50%, 20%, 10%, 5%, 2%, 1%. This test case allows very simply to check the photometric capability of the reconstruction. Source 5 is a simple example of a perfectly point-symmetric and resolved object. Finally source 6 is almost symmetrical, except for a star component to test for cases where the symmetric part of the object is well reconstructed but not the asymmetric one.

Once the test target has been selected, target visibilities are straightforwardly computed at all uv points (given by the telescope configuration and the observation time). Then these visibilities are used to derive the powerspectrum and bispectrum data. Noise is added to these last quantities. In practice we introduced independently some noise on the visibility amplitudes and on the visibility phases. As expected long baseline data had poorer SNR than shorter ones. The noise levels were defined as 0.2%, 2%, 5%, 10% and 20% for the visibility errors, and 0.1°, 1.0°, 3.0°, 6.0° and 12.0° errors for the closure phases on the shortest baselines. For each telescope configuration and source, 50 fake observations were simulated, each differing by its noise realization.

3.2 Reconstruction process

The pixellation of the reconstructed images was chosen equal to that of the source. The starting model for all images was a default Gaussian function centered in the field of view, with a FWHM of 2.0 mas.

To evaluate the fidelity of a reconstructed image $\widehat{\boldsymbol{I}}$ with respect to the source $\boldsymbol{O}$, they were first aligned by cross-correlation, then the Mean Squared Error was computed. When considering a whole data set, composed of images only differing by their noise occurrences, the actual error was computed as the square root of the averaged MSE. Several noise realizations were also needed to compute the standard deviation over a set (all parameters fixed, the standard deviation of the individual errors measures the repeatability of the algorithm at a determined noise level: this constitutes a good indicator of the confidence the user can have in the reconstruction at this noise level; the lower the standard deviation, the more trustworthy the reconstruction is).

4. SIMULATION RESULTS

As we cannot publish here the reconstructions for all targets and all array configurations, the following sections present only the most representative results. The reader is invited to download a complete report on those simulations to BSMEM webpage,[11] which contains a more detailed analysis of the simulations.

4.1 Performance with noise

Fig. 4 presents the reconstructions obtained on four sources for low, medium, and high noise on the visibility amplitudes and closure phases.

At high and medium SNR on both noise parameters, BSMEM is always able to retrieve at least the main features of all targets. Of course the better the uv coverage is, the better the reconstruction gets (see next section), but both noises do also play major role. Reconstructions behave as expected: noisier data sets produce poorer reconstructed images, and sources that exhibit extended components are more difficult to reconstruct at high noise.

Let us consider the reconstructions corresponding to a constant noise level on the phase, e.g. 1°. At high SNR on the visibility amplitudes, BSMEM is initially able to reconstruct the image with fine details. Then as the level of amplitude noise increases, there is a typical loss of details, and the reconstructions appear more and more blurry. This is particularly visible on the "Symmetric stars" object (bottom right in each frame). While the noise on the amplitudes remains low, both stars still appear well separated. As soon as the amplitudes get noisier, their respective disks blend. Finally above a certain threshold the reconstruction of the target is not possible anymore: the data is not informative enough to depart significantly from the starting model. Similarly the spots on the "Star + spots" becomes increasingly difficult to distinguish.

The reconstruction behavior is different when the phase noise is increased while the amplitude noise is kept constant. In this case, although the reconstructed image gets visibly noisier, this does not prevent the target from being partially reconstructed (the algorithm does depart from the prior). The effect of noise on the reconstructed images is also different: all features remains in the image and there is nearly no smoothing. However the images are "spread" with visible noise artifacts inside the whole field of view.

The common interpretation is that the powerspectrum data determine the amount of flux in the reconstructed image and the overall shape of the source while the closure phases constrain the flux localisation, allowing to retrieve finer details. Noisier phases lead the reconstruction process into putting flux at the wrong locations, explaining the noise repartition on the whole image. At worse the reconstruction proceed as if there was no

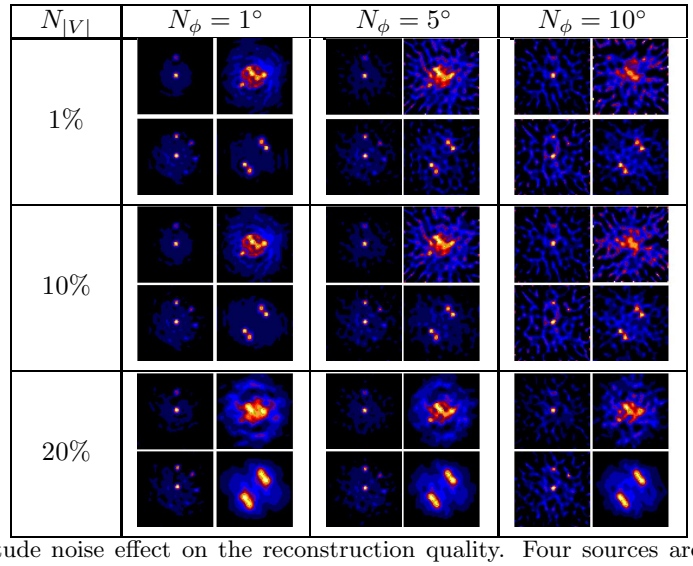

Figure 4. Phase and amplitude noise effect on the reconstruction quality. Four sources are reconstructed for different phase and amplitude noise images (objects 1, 3, 4, 5) are reconstructed 8 telescopes..

information on the phase, and then it is likely to retrieve a symmetrised version of the target. On the contrary very noisy amplitudes with good closures prevent BSMEM from even retrieving the global shape of the target, but the flux is still constrained within an area, creating a blurring effect.

Maybe quite paradoxally, as both noises alter the image in opposite ways, having more noise might improve the visual quality of an image. For example, for high level of amplitude noise (20%), images with low phase noise are less detailed than images with medium phase noise.

Our other simulations (not shown here) agree in that there is always a clear degradation of the confidence level (the standard deviation of the reconstruction errors) when the visibility noise increases, while it reaches a plateau for the phase noise.

Keeping fixed the amplitude noise level, there is also a threshold of phase noise under which the error stays constant. This means that even good closure phases will not bring any improvement to image quality when the powerspectrum are of poor quality.

4.2 Influence of the *uv* coverage

As Fig. 5 demonstrates, the 15 telescope *uv* coverage gives nearly perfect images, and point source targets are particularly well rendered. In comparison, on other configurations a certain amount of ghost flux appears around the stars, slowly increasing as the *uv* coverage gets worse. The stars themselves are not point-like anymore, though both components can perfectly be distinguished and are of the correct flux ratio. This situation remains unchanged on the resolved binary (note that other simulations show that high SNR phases are more important than high SNR amplitudes in order to distinguish the weakest star).

The reconstruction of low level intensities is much harder with poorer *uv* coverage, as underlined by the "star+spots" source reconstructions: BSMEM successfully manages to recover 5-7 of the 7 stars with 15 telescopes, 4-7 with 8 telescopes, 3-7 with the 6 telescope one, and 3 to 4 for the 4 telescope one. As the star fluxes follow a progression of 50%, 20%, 10%, 5%, 2%, 1% for this object, this roughly translates into doubled reconstruction sensitivity when going from the 4 telescope array to the 6, 8 and finally to the 15 one.

It should be noted that high phase noise alone can severely degrade the performance of an array, even decreasing its sensitivity down to the level of a smaller array. At the same level of noise on visibility amplitudes, a 4 telescope array with high SNR closure phases can perform better than a 6 telescope one with low SNR. This is a strong advocacy for decent SNR on closure phases and also reassuring for VLTI imaging using solely the UTs.

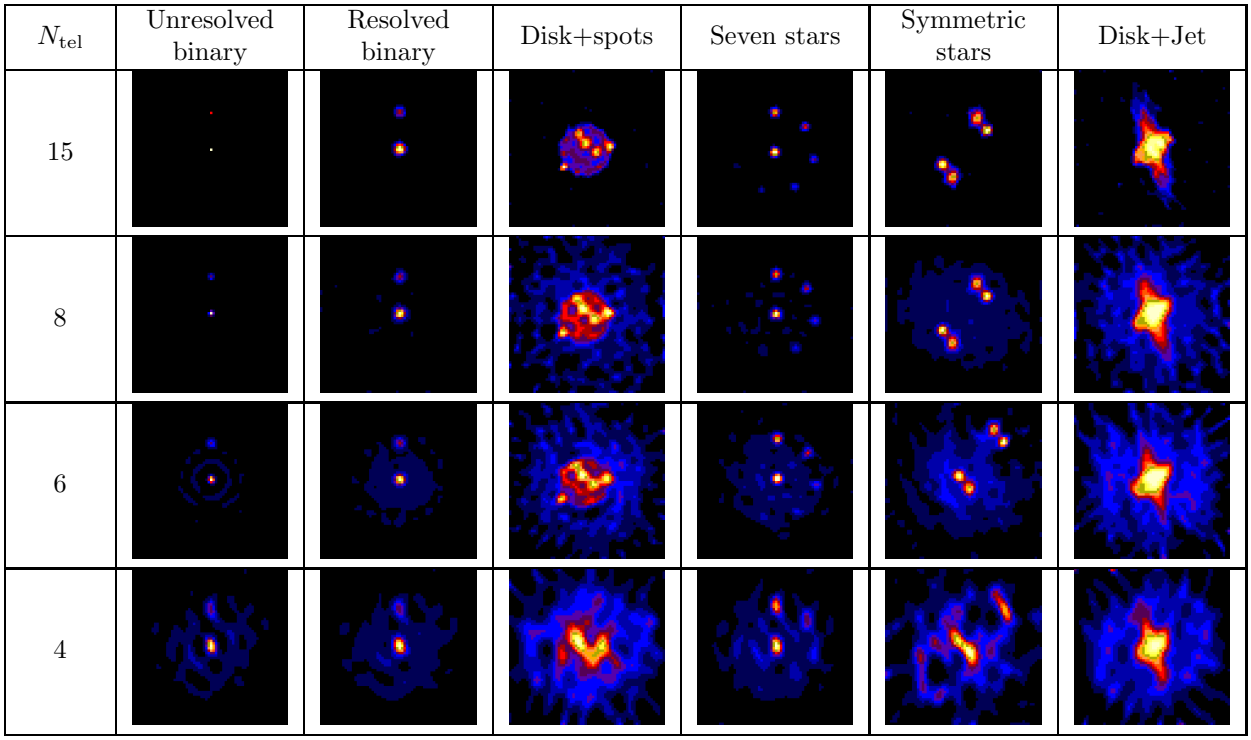

Figure 5. Evolution of the reconstructions with the UV coverage. These simulations were realised at medium SNR on the amplitudes and phases.

Furthermore, even if true model-independent imaging is reputed to be difficult with only a 4 telescope array, it should be noted that it generally succeeds in retrieving the main features of all targets. Model-fitting should then allow to retrieve most of the scientific information. The "Star+spots" source is the one where this main feature – the central background disk – is the faintest compared to its other components and where the major improvement is brought by going from 4 to 6 telescopes. The 4 telescopes array can clearly reconstruct the bright spots, but not the disk itself even at high SNR, while the 6 telescopes array can at medium SNR. Note that this is not due to the greater *uv* coverage for the same amount of time, but mainly to the more complete phase information held by the bispectrum data (see next section). The 8 and 15 configurations further improves the results, reconstructing the object with the right shape even with low SNR phases.

Finally the images of the most symmetric sources, "Symmetric stars" and "Disk+Jet", underline the difficulty to reconstruct objects on which phases do not bring much useful information. On those objects the influence of *uv* coverage is less relevant than the quality of the phase measurements. We carried out further simulations at high phase noise which showed even the 15-telescope configuration unable to retrieve correctly the "Disk+Jet" target.

5. POWERSPECTRUM AND BISPECTRUM INFLUENCE

We discussed in a previous paper how reconstructions can be severely affected by missing bispectrum.[12] To simulate missing bispectrum we reconstructed images with only a subset of the bispectrum or powerspectrum. In a real interferometer, bispectrum points are expected to be more difficult to acquire than powerspectrum, so we concentrate here on the results obtained when using the full set of powerspectrum data and 0%, 25%, 50%, 75%, 100% of the available bispectrum data. The simulations were done for three noise levels on both the powerspectrum and bispectrum: low SNR data ($> 20\%$ powerspectrum errors, $> 20°$ closure phases), medium SNR data (about 10% powerspectrum errors, about 10° closure phases), and high SNR data (1% powerspectrum errors, 1° closure phases).

As expected, when the noise levels of the bispectra and the powerspectra are homogeneous (both low, medium or high), the reconstruction error are decreasing with the bispectra and powerspectra utilisation percentages. Fig. 6 is a typical example. Purely from the viewpoint of feature, on this source (and for most other sources at medium SNR) a plateau of performance is reached after the 50% threshold. i.e. in most practical cases less than 50% of bispectrum are really needed when the other type of data is fully available.

Our simulations tackled the issue of the usability of low SNR data, and they demonstrated that the Bayesian approach ensures that all data points are useful. On Fig. 6 a constant improvement in reconstruction quality is noted for both sources when low SNR bispectrum are progressively added to high SNR powerspectrum. Although is still widely believed by some interferometrists that very noisy data should be discarded, this is a remnant of a time when non-Bayesian algorithms such as CLEAN were used, in which the noise was improperly treated. When using the current generation of image reconstruction software and adding powerspectrum to a full set of bispectra (whichever their SNR), performance is improved overall. Similarly even if added bispectra are noisier than the corresponding powerspectrum, they nonetheless still bring useful information, both on the phase and on the amplitude (through the triple amplitude). This point is to keep in mind when very few bispectrum points are available on an object and are known to be extremely noisy.

When the SNR discrepancy between the bispectrum and powerspectrum is small, their relative influence in the success of a reconstruction depends mainly on the amount of symmetry of the observed target. As visibilities for a point-symmetric object are real, the information bispectrum points provide is very small, i.e. the triple amplitudes. Simulation results on the most centrosymmetric object show that reconstructions using mainly powerspectrum always give better performance than those using mainly bispectrum. Thus one might think powerspectrum on its own is enough to reconstruct point-symmetric sources, and that bispectrum data become relevant only when the target is asymmetric. However such statements are based on the assumption that you know the degree of symmetry of your source, which is only possible if any least some phases have been secured on this target or if the target shape was already partially known. As shown previously, datasets containing predominantly powerspectrum but with a few bispectrum data points contains often enough information about the source asymmetries to ensure a correct reconstruction. Therefore in general the powerspectrum data can be considered as an indication of the amount of flux present in the symmetrized object, while the bispectrum provides the exact localisation of this flux in its non-symmetric parts.

The problem of reconstruction from powerspectrum-only data is mathematically undetermined so that both the image of the target and its symmetric can be indifferently retrieved. In several simulations using very few bispectrum points (0% and 25%), we determined that the reconstructed image was a superposition of the source with its symmetric. Even a full *uv* coverage was unable to prevent this effect. A decent amount of bispectrum is definitively required to remove the symmetry ambiguity which exists in non point-symmetric targets. As more bispectrum are used, this ambiguity is progressively lifted. That's why in most practical cases, a reconstruction using mostly powerspectrum plus a few bispectrum is roughly equivalent performance-wise to a reconstruction using mostly bispectrum plus a few powerspectrum.

6. CONCLUSION

We have presented several simulation assessing the capabilities of our image reconstruction software BSMEM when reconstructing from noisy datasets or with incomplete bispectrum coverage.

Although our test targets may be considered difficult cases, the presented model-independent reconstructions have been successful for the typical noise levels of current facilities. As expected the image quality mostly depends on the*uv* coverage.

Reconstruction with a poor *uv* coverage (4 telescopes) is difficult but still possible for most objects. The acquisition of bispectrum data is of primary importance for actual performance of model-independent reconstructions, and achieving an adequate sampling of decent quality bispectra is arguably more important than a simple increase in the number of telescopes. With excellent SNR on the data and enough time, 4 telescope array would be generally sufficient for the simplest targets, and a 6 telescope one would generally produce images including all features of moderately difficult sources. Compared to the ideal situation of a 15 telescope interferometer, the 6 and 8 telescope cases lead to noisier reconstructions. However even at medium signal-to-noise, they allow to

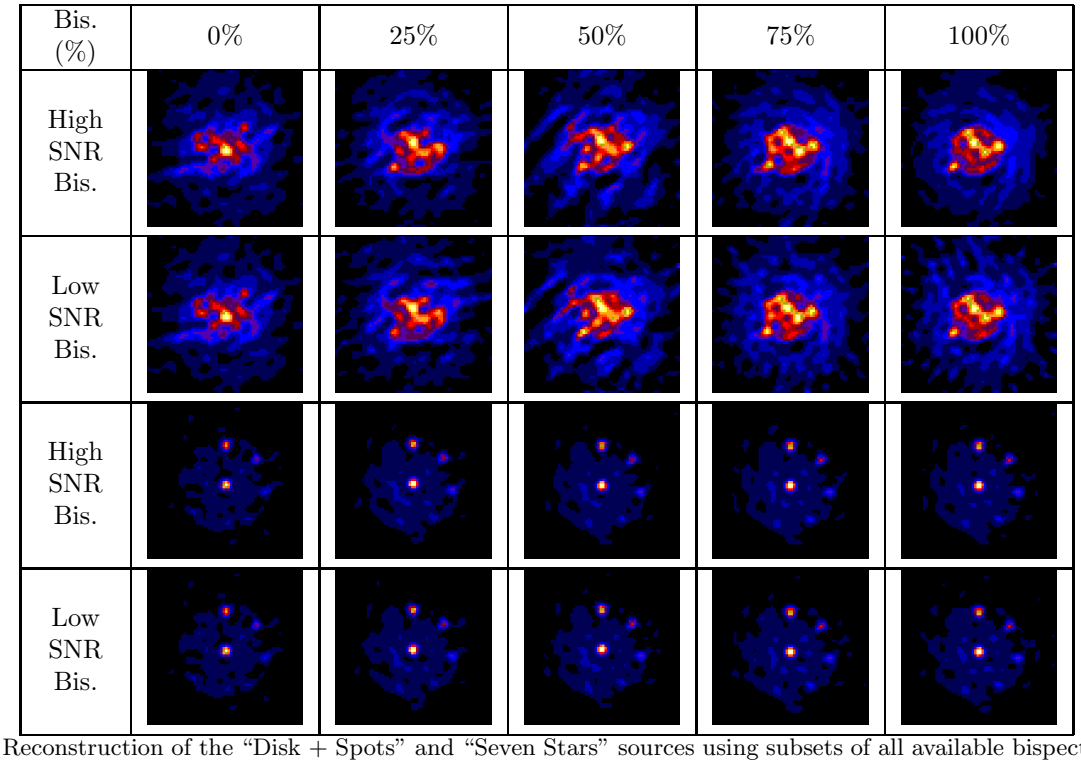

Figure 6. Reconstruction of the "Disk + Spots" and "Seven Stars" sources using subsets of all available bispectrum data, with high SNR powerspectra and the 6-telescope array configuration. Whether the bispectra are of high or low SNR powerspectrum, the image quality of the reconstruction is visibly improved up to 75%.

retrieve all the features of the sources. The 8 telescope array is particularly impressive in this regard: nothing but a slight noise reduction is gained from adding other stations.

Requirements on bispectrum and powerspectrum coverage vary with the nature of the observed target. The reconstruction error is not always a decreasing and monotonous function of the bispectrum percentage. A reconstruction with optimal bispectrum coverage but average *uv* coverage may indeed be superior to another with better *uv* coverage but with poorer bispectrum sampling. Closure phases of reasonable SNR are generally sufficient, and contrary to the intuition, closure phases of much higher SNR than the powerspectrum do not necessarily improve the reconstruction by a substantial amount.

Moderate noise on closure phases rarely prevents a successful reconstruction, so that the brightest components of the targets or at least its global shape can still be identified. Noise on visibility amplitudes, though, strongly degrades the performance, up to a point where convergence is hard to achieve. The image quality offered by a 6 telescope array at low SNR is very similar to that of a 4 telescope array at medium SNR.

Consequently the challenge for next-generation inteferometers will be to obtain high SNR measurements while increasing *uv* coverage. Future facilities such as MROI are oriented toward these goals, and they should definitively bring imaging into the foreground of interferometry.

ACKNOWLEDGMENTS

We would like to thank the the JRA4 of the Integrated Infrastructure Initiative OPTICON that funded a part of this research. We also acknowledge support provided by the Particle Physics and Astronomy Research Council for our ongoing research at the Cavendish laboratory. Finally the authors would like to thank S.F. Gull and the team of MEDC Ltd for their support on MEMSYS libraries and the provided documentation.

REFERENCES

[1] Lawson, P. R., Cotton, W. D., Hummel, C. A., Monnier, J. D., Zhao, M., Young, J. S., Thorsteinsson, H., Meimon, S. C., Mugnier, L., Le Besnerais, G., Thiebaut, E., and Tuthill, P. G., "The 2004 Optical/IR Interferometry Imaging Beauty Contest," in [*Bulletin of the American Astronomical Society*], *Bulletin of the American Astronomical Society* **36**, 1605–+ (Dec. 2004).

[2] Lawson, P. R., Cotton, W. D., Hummel, C. A., Baron, F., Young, J. S., Kraus, S., Hofmann, K.-H., Weigelt, G. P., Ireland, M., Monnier, J. D., Thiébaut, E., Rengaswamy, S., and Chesneau, O., "2006 interferometry imaging beauty contest," in [*Advances in Stellar Interferometry. Edited by Monnier, John D.; Schöller, Markus; Danchi, William C.. Proceedings of the SPIE, Volume 6268, pp. 62681U (2006).*], *Presented at the Society of Photo-Optical Instrumentation Engineers (SPIE) Conference* **6268** (July 2006).

[3] Meimon, S. C., Mugnier, L. M., and Le Besnerais, G., "A novel method of reconstruction for weak-phase optical interferometry," in [*New Frontiers in Stellar Interferometry, Proceedings of SPIE Volume 5491. Edited by Wesley A. Traub. Bellingham, WA: The International Society for Optical Engineering, 2004., p.909*], Traub, W. A., ed., *Presented at the Society of Photo-Optical Instrumentation Engineers (SPIE) Conference* **5491**, 909–+ (Oct. 2004).

[4] Meimon, S. C., Mugnier, L. M., and Le Besnerais, G., "Reconstruction method for weak-phase optical interferometry," *Optics Letters* **30**, 1809–1811 (July 2005).

[5] Ireland, M. J., Monnier, J. D., and Thureau, N., "Monte-Carlo imaging for optical interferometry," in [*Advances in Stellar Interferometry. Edited by Monnier, John D.; Schöller, Markus; Danchi, William C.. Proceedings of the SPIE, Volume 6268, pp. 62681T (2006).*], *Presented at the Society of Photo-Optical Instrumentation Engineers (SPIE) Conference* **6268** (July 2006).

[6] Buscher, D. F., "Direct maximum-entropy image reconstruction from the bispectrum," in [*Very High Angular Resolution Imaging*], Robertson, J. G. and Tango, W. J., eds., *IAU Symposium* **158**, 91–+ (1994).

[7] Gull, S. F. and Skilling, J., "Quantified Maximum Entropy - Memsys5 Users' Manual," *Maximum Entropy Data Consultants Ltd., South Hill, 42 Southgate Street, Bury St. Edmunds, IP33 2AZ, United Kingdom* (1991).

[8] Maximum Entropy Data Consultants Ltd. website: `http://www.maxent.co.uk`.

[9] Pauls, T. A., Young, J. S., Cotton, W. D., and Monnier, J. D., "A Data Exchange Standard for Optical (Visible/IR) Interferometry," *The Publications of the Astronomical Society of the Pacific* **117**, 1255–1262 (Nov. 2005).

[10] Thureau, N. D., Ireland, M., Monnier, J. D., and Pedretti, E., "Software tools for optical interferometry," in [*Advances in Stellar Interferometry. Edited by Monnier, John D.; Schöller, Markus; Danchi, William C.. Proceedings of the SPIE, Volume 6268, pp. 62683C (2006).*], *Presented at the Society of Photo-Optical Instrumentation Engineers (SPIE) Conference* **6268** (July 2006).

[11] BSMEM webpage: `http://www.mrao.cam.ac.uk/research/OAS/bsmem.html`.

[12] Thorsteinsson, H., Buscher, D. F., and Young, J. S., "The bispectrum in model-independent imaging," in [*New Frontiers in Stellar Interferometry, Proceedings of SPIE Volume 5491. Edited by Wesley A. Traub. Bellingham, WA: The International Society for Optical Engineering, 2004., p.1574*], Traub, W. A., ed., *Presented at the Society of Photo-Optical Instrumentation Engineers (SPIE) Conference* **5491**, 1574–+ (Oct. 2004).